Broadband Polarization Beam Splitter Rotator Using Only Silicon Nitride

Fatemeh Ghaedi Vanani 1,2, Alireza Fardoost¹, Guifang Li¹, and Christopher Doerr²

¹CREOL, The College of Optics and Photonics, University of Central Florida, Orlando, FL 32816, USA

²Aloe Semiconductor, Middletown, NJ 07748, USA

Fatemeh.GhaediVanani@ucf.edu

Abstract: We designed and fabricated a CMOS-compatible polarization beam splitter and rotator purely in Si_3N_4 , achieving experimentally an insertion loss of ~1.5dB and a polarization extinction ratio greater than 15dB from 1280 to 1320nm. ©2024 The Authors

1. Introduction

In the past few years, controlling and manipulating the polarization in photonic integrated circuits (PICs) have become very important. Polarization splitters and polarization rotators are two fundamental components widely used in optical communications including dual-polarization transmitters and receivers, in both coherent and direct-detection systems. There have been many demonstrations of polarization rotators/splitters on the silicon-on-insulator (SOI) platform [1], but the need for high aspect ratio features makes them incompatible with commercial foundry processes [2]. Silicon nitride (Si₃N₄) waveguides, on the other hand, are less sensitive to edge roughness, are more tolerant to fabrication variations [3], and can handle much higher optical power than silicon waveguides. Therefore, Si₃N₄ proves to be a better CMOS-compatible material for many passive components compared with silicon and is a promising candidate for photonic device applications with ultra-low propagation loss spanning from visible to near-infrared wavelengths using devices including grating couplers, micro-resonators, and polarization rotation/splitters [3].

There are many different techniques to implement an on-chip polarization beam splitter such as Mach-Zehnder interferometers [4], multimode interference (MMI) structures [5], and directional couplers [6]. Among these structures, MMI couplers have the advantage of low loss. However, they come with the trade-off of requiring a very large footprint because the length of the MMI coupler must be an integer multiple of the beat length of both TE and TM polarizations. On the other hand, asymmetric directional couplers (ADC) have the advantage of a very high polarization extinction ratio (RER) but they have limited operation bandwidth because of their wavelength-sensitive coupling length [7]. In both cases, the TM0 input remains in the same mode, resulting in significant device limitations.

Here, we present a polarization beam splitter and rotator (PBSR) designed for the Si₃N₄ material platform with broadband operation from 1260nm-1360nm, combining both splitter and rotator functionalities. Using only Si₃N₄, leads to significantly improved power handling on the chip compared to silicon waveguides, mainly due to two-photon absorption (TPA) effects in silicon. While a few PBSRs have been demonstrated in Si₃N₄ [8], to the best of our knowledge, there is no report of a PBSR exclusively using Si₃N₄ in the O-band. Si waveguides exhibit significantly higher TPA in the O-band than the C-band, with TPA effects becoming notable at powers as low as 4 mW [9]. In addition, the previously reported PBSR utilized 400nm thick Si₃N₄, typically resulting in higher polarization-dependent loss (PDL) when coupling to optical fiber. Our proposed PBSR comprises only a 300nm thick Si₃N₄ layer with SiO₂ cladding on top and bottom, with a combination of fully and partially etched levels which puts significantly less burden on the process and allows much higher power handling capability and lower PDL for fiber coupling. Also, having the PBSR obviates the need to couple TM between Si₃N₄ and Si, which generally has a lower coupling efficiency.

First, using two bi-level tapers with different tapering slopes, the fundamental TM mode (TM0) is converted into a first-order TE mode (TE1) to increase the effective index difference. Next, TE0 and TE1 modes are split by using an asymmetric adiabatic coupler. The experimental results demonstrate the insertion loss of ~1.5dB and the PER better than 18dB and 15dB for TE0 and TM0 modes, respectively, for 60nm bandwidth from 1260nm-1320nm. The design is adiabatic and thus very broadband and tolerant to fabrication changes.

2. Device Structure

Figure 1(a) shows the schematic of our proposed PBSR. In this design, we utilized two etched levels for the Si_3N_4 waveguide: a fully-etched level (300nm, rib) and a partially-etched level (180nm, slab). In Fig.1(a), brown and red colors represent fully etched and partially etched regions, respectively. Our PBSR design consists of three main sections. In the first section, employing two bi-level tapers with different slopes for the slab, the TM0 mode is converted into the TE1 mode while maintaining a constant rib waveguide width of $0.4\mu m$. We employed the finite-difference eigenmode method (FDE, Lumerical Inc.) to calculate the effective indices for the first three eigenmodes of the Si_3N_4 rib waveguide. This calculation was performed for different slab widths (W_8) while the rib width (W_8)

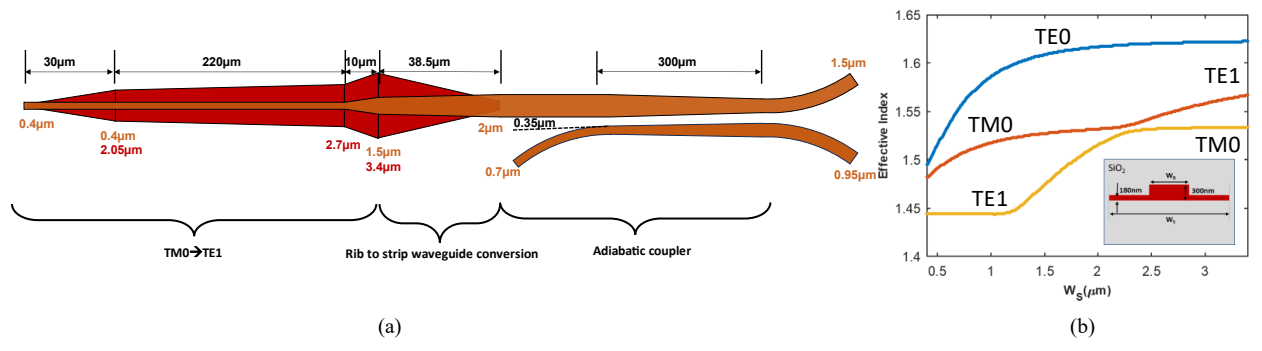


Fig. 1: (a) Schematic of the polarization beam splitter rotator (PBSR). The red represents the 300nm-thick Si₃N₄ while brown indicates the 180nm partially etched slab. (b) The effective indices of the first three eigenmodes of the rib waveguide at the wavelength of 1310nm. Here, the rib width (W_R) remains constant at 0.4μm.

remains constant at $0.4\mu m$, at the center wavelength of 1310nm, as shown in Fig.1 (b). The partially-etched waveguide is vertically asymmetric which makes the mode conversion between the TM0 and TE1 mode possible even with the same material for the upper-cladding and under-cladding, because it splits the hybrid modes [10]. Also, the bi-level waveguide makes a large effective index difference between modes TM0 and TE1 through the structure as shown in Fig.1(b). This keeps the TM0 input in mode 2 through the bi-level taper at first evolving into a hybridized TM0-TE1 mode and then converting into the TE1 mode. The TE0 input mode remains unchanged during the propagating through the tapers and exits as TE0 mode.

In the second section, the rib waveguide width (W_R) starts to widen while the slab width (W_s) narrows, eventually converting the rib waveguide into a strip waveguide $2\mu m$ wide. In the final section, a narrow strip waveguide with $0.7\mu m$ width is placed next to the wide waveguide with 350nm gap. By using this asymmetric adiabatic coupler, the TE1 mode in the wide waveguide couples to the TE0 mode in the adjacent narrow waveguide. Meanwhile, the TE0 mode of the wide waveguide remains within it through the adiabatic coupler due to the phase mismatch. With this, TE0 and TM0 modes at the input are separated with a high extinction ratio while also the TM0 mode is converted into the TE0 mode at the output.

3. Simulation

We optimized the width and length of each section using an eigenmode Expansion (EME) solver, and then calculated the PER and insertion loss of the entire PBSR using the finite-difference time-domain (FDTD) method. Figure 2 (a) shows electric field evolutions of the TE0 and TM0 modes at the input of the PBSR, as well as the transverse mode profiles of the first and second highest effective indices at different locations along the PBSR. The field distributions closely matched the expected device performance, effectively illustrating both splitting and rotation processes through wave propagation. The transmission spectra of the TE0 and TM0 mode at the input, as found from FDTD simulation, are depicted in Fig.2 (b), representing an insertion loss of less than 0.4dB and the PER exceeding -26dB over a 100nm bandwidth, ranging from 1260 to 1360nm.

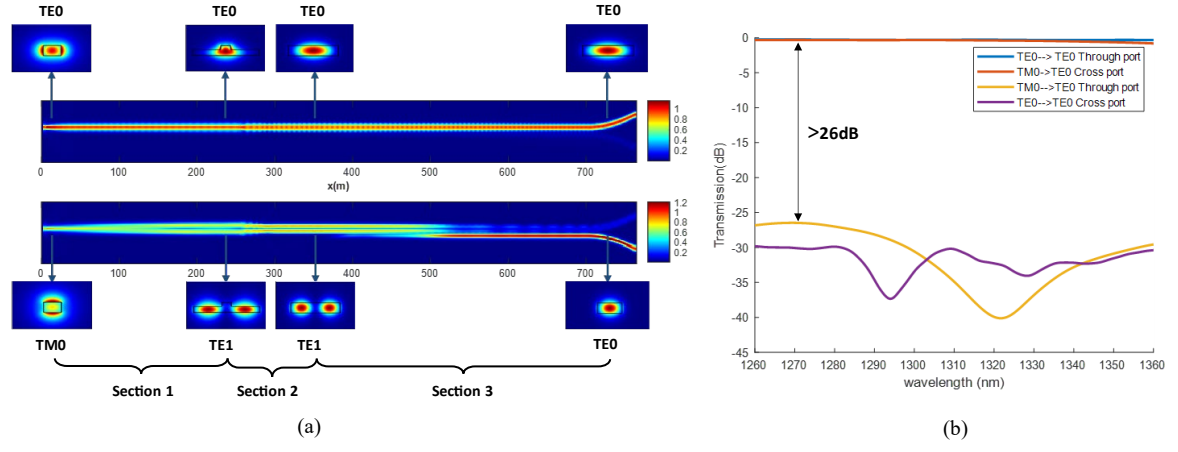


Fig. 2: (a) The electric field propagations of the TE0 and TM0 modes at the input of the PBSR, along with the transverse mode profiles of the first and second highest effective indices at different locations of the designed PBSR. (b) Transmission spectra of the TE0 and TM0 input modes through the PBSR using FDTD simulation.

4. Fabrication and measurement

The proposed design was fabricated at AMF using a SOI wafer with $2\mu m$ buried oxide layer (BOX) and $6\mu m$ silica upper cladding deposition. The optical micrograph of the fabricated PBSR is shown in Fig. 3(a) where the input and outputs of the PBSR are directed towards the edge couplers. We evaluated the performance of the PBSR by coupling light from a tunable laser covering wavelengths of 1260-1360nm, in and out of the PBSR chip via a fiber array. The optical power at each wavelength was measured using a power meter. Additionally, we employed a back-to-back reference single-mode waveguide to characterize the TE and TM transmissions through the edge couplers to find the on-chip loss, as shown in Fig. 3(a).

The measurement results are presented in Fig. 3(b). The TE polarization output is extracted from the through port and the TM polarization output is obtained from the cross port, as shown in Fig. 3(a). At the cross port, the PER exceeds 18dB over the entire bandwidth range from 1260 to 1360nm. Meanwhile, at the through port, the PER is better than 15dB for the wavelength range of 1260-1320nm. The transmission results exclude the coupling loss between the fiber array and the waveguide facets. Consequently, the on-chip loss of the PBSR is approximately 1.5dB for both TE0 and TM0 modes across the wavelength range 1260-1320nm, considering a ± 0.5 dB coupling error. The measured insertion loss is higher, and PERs are lower than the corresponding simulation results particularly for longer wavelengths, mainly due to fabrication imperfections such as variations in Si₃N₄ rib and slab thickness. The fabrication process has been modified for our next run and improved insertion loss and PER are expected.

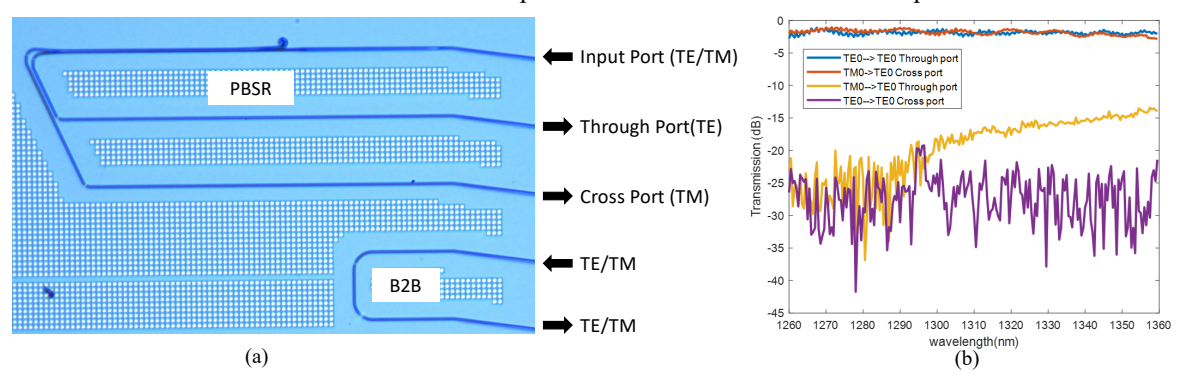


Fig. 3: (a) The optical micrograph of the fabricated PBSR. (b) Measured transmission spectra for TE0 and TM0 modes at the through and cross ports of the PBSR.

5. Conclusion

In this paper, we designed and experimentally demonstrated a novel polarization beam splitter rotator entirely in silicon nitride. It has an overall insertion loss of ~1.5dB and a PER larger than 15dB in the O-band, where TPA is a much more significant issue in silicon waveguides than in the C-band. The device is CMOS foundry compatible and works with silica over cladding which is required for photonic integrated circuit packaging.

This work was supported in part by the Army Research Office under contracts W911NF-23-1-0197 and NSF under grant numbers ECCS-1932858.

6. References

- 1. Sacher, W.D., et al., Polarization rotator-splitters in standard active silicon photonics platforms. Optics express, 2014. 22(4): p. 3777-3786.
- 2. Dai, X., Q. Lu, and W. Guo. Fabrication-tolerant polarization rotator-splitter based on silicon nitride platform. in Optical Fiber Communication Conference. 2021. Optica Publishing Group.
- 3. Sharma, T., et al., Review of recent progress on silicon nitride-based photonic integrated circuits. Ieee Access, 2020. 8: p. 195436-195446.
- Liang, T.K. and H.K. Tsang, Integrated polarization beam splitter in high index contrast silicon-on-insulator waveguides. IEEE photonics technology letters, 2005. 17(2): p. 393-395.
- Yin, M., et al., CMOS-compatible and fabrication-tolerant MMI-based polarization beam splitter. Optics Communications, 2015. 335: p. 48-52.
- Errando-Herranz, C., S. Das, and K.B. Gylfason, Suspended polarization beam splitter on silicon-on-insulator. Optics Express, 2018. 26(3): p. 2675-2681.
- 7. Tian, Y., et al., Compact polarization beam splitter with a high extinction ratio over S+ C+ L band. Optics Express, 2019. 27(2): p. 999-1009.
- 8. Dai, X., et al. High Performance Polarization Rotator-Splitter Based on Si 3 N 4 Waveguide with Relaxed Fabrication Tolerance. in 2022 European Conference on Optical Communication (ECOC). 2022. IEEE.
- Suzuki, K., et al., Strictly non-blocking 8×8 silicon photonics switch operating in the O-band. Journal of Lightwave Technology, 2020. 39(4): p. 1096-1101.
- Dai, D., Y. Tang, and J.E. Bowers, Mode conversion in tapered submicron silicon ridge optical waveguides. Optics express, 2012. 20(12): p. 13425-13439.